

Article

A Simple and Sustainable Prediction Method of Liquefaction-Induced Settlement at Pohang Using an Artificial Neural Network

Sung-Sik Park ¹, Peter D. Ogunjinmi ¹ , Seung-Wook Woo ¹ and Dong-Eun Lee ^{2,*}

¹ Department of Civil Engineering, Kyungpook National University, 80 Daehakro, Bukgu, Daegu 41566, Korea; sungpark@knu.ac.kr (S.-S.P.); ogunjinmipeter@gmail.com (P.D.O.); geowsw@knu.ac.kr (S.-W.W.)

² Department of Architectural Engineering, Kyungpook National University, 80 Daehakro, Bukgu, Daegu 41566, Korea

* Correspondence: dolee@knu.ac.kr; Tel.: +82-53-950-7540

Received: 8 April 2020; Accepted: 9 May 2020; Published: 13 May 2020



Abstract: Conventionally, liquefaction-induced settlements have been predicted through numerical or analytical methods. In this study, a machine learning approach for predicting the liquefaction-induced settlement at Pohang was investigated. In particular, we examined the potential of an artificial neural network (ANN) algorithm to predict the earthquake-induced settlement at Pohang on the basis of standard penetration test (SPT) data. The performance of two ANN models for settlement prediction was studied and compared in terms of the R^2 correlation. Model 1 (input parameters: unit weight, corrected SPT blow count, and cyclic stress ratio (CSR)) showed higher prediction accuracy than model 2 (input parameters: depth of the soil layer, corrected SPT blow count, and the CSR), and the difference in the R^2 correlation between the models was about 0.12. Subsequently, an optimal ANN model was used to develop a simple predictive model equation, which was implemented using a matrix formulation. Finally, the liquefaction-induced settlement chart based on the predictive model equation was proposed, and the applicability of the chart was verified by comparing it with the interferometric synthetic aperture radar (InSAR) image.

Keywords: settlement; artificial neural network; liquefaction

1. Introduction

The Pohang earthquake ($M_w = 5.4$) that struck the Heunghae Basin, around Pohang City, on 15 November 2017, had a damaging effect, leading to liquefaction and lateral spreading. Since the event, several attempts have been made to study the post-earthquake damage [1–5]. However, little attention has been paid to the settlement resulting from the liquefaction. This study tried to predict the liquefaction-induced settlement of Pohang by applying a machine learning algorithm to a standard penetration test (SPT) data and proposes a liquefaction settlement chart based on the results. Before constructing a structure on the ground, design is performed based on the ground investigation results. In addition, many sites, including Pohang, have a lot of SPT data. The SPT is a common method to get ground investigation data.

Assessing liquefaction-induced settlements is a major challenge in geotechnical earthquake engineering since a variety of phenomena such as re-sedimentation or reconsolidation (volumetric strain) of the liquefied soil, ground loss due to venting of liquefied soil (i.e., sand boils or ejecta), lateral spreading under zero volume change, soil-structure interaction ratcheting, and bearing capacity failure are associated with them [6]. For numerical analysis, earthquake-induced liquefaction in the free-field can be interpreted as a 1D phenomenon occurring along a vertical soil column in which earthquake-induced cyclic shear and compressive forces increase the pore pressure and thereby cause

a reduction in the transient stiffness and strength of the soil. After liquefaction, reconsolidation occurs in the soil owing to the dissipation of the excess pore pressure (Δu) by means of water flow, and it results in the vertical settlement of the ground surface [7].

Tang et al. [8] classified the significant parameters controlling seismic soil liquefaction into seismic parameters, site conditions, and soil parameters. Out of 22 influence factors, they identified 12 as being significant, and they were the magnitude, epicentral distance, duration, fines content, particle size, grain composition, relative density, drainage condition, degree of consolidation, thickness of the sand layer, depth of the sand layer, and groundwater table. Over the years, researchers have considered some of these significant influence factors for predicting earthquake-induced liquefaction and its effects through machine learning techniques [9,10].

Therefore, simple artificial neural network (ANN) models were adopted to predict liquefaction-induced settlement on the basis of SPT database from the Korea Geotechnical Information DB system [11] and the Pohang earthquake. In the following sections, the research methodology and findings are presented.

2. Motivation and Study Objective

Liquefaction-induced settlement is often calculated by considering numerous parameters and following several complex analytical and numerical procedures. However, obtaining such parameters in the field may not be practicable in most cases, as some of the required data may not be available. Hence, there is a need for an alternative simple settlement prediction procedure that requires a few parameters that are readily obtained from a field observations database. Therefore, the objective of this study is to fill this gap by presenting a tool to predict liquefaction-induced settlement that may occur when an earthquake occurs in the field using SPT data obtained in the past.

3. Methodology

The database used in this study was collected from the Korea Geotechnical Information DB system [11] and the UBCSAND constitutive effective stress model [12]. Through a 1D column analysis, the UBCSAND model estimates the shear-induced deformation from SPT data and earthquake information. SPT data were obtained for five different borehole sites near the epicenter of the earthquake at Pohang. The summary statistics of the data set are presented in Table 1 and the details of the database are in Table A1.

Table 1. Summary statistics of the data set.

	Input Parameters				Output
	Depth (m)	Unit Weight (kN/m ³)	$N_{1(60)}$	CSR	Settlement (mm)
Count	100	100	100	100	100
Mean	10.500	18.960	13.620	0.314	0.898
Std.	5.795	1.869	8.722	0.045	0.874
Min.	1	16	0	0.21	0
25%	5.75	18	7	0.29	0.3
50%	10.5	20	11	0.32	0.6
75%	15.25	21	25	0.34	1.4
Max.	20	21	25	0.39	3.4

The data set comprised 100 data points (20 data for each borehole) along with the corresponding settlement values. The locations of the boreholes considered in the study are shown in Figure 1.

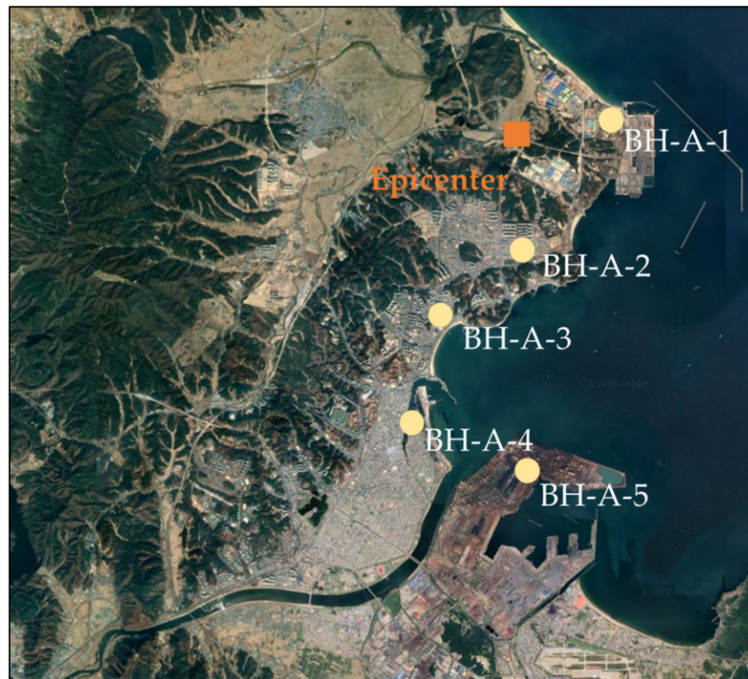


Figure 1. Locations of boreholes in Pohang City considered in this study.

3.1. Data Division and Preprocessing

The settlement prediction process comprises training and testing. Seventy percent of the entire data set was used for training, and the remaining 30% was used for testing. The data were preprocessed before training the algorithm, to ensure quick convergence and minimize the generalization error. This involved scaling the input variables to the range -1 to $+1$ by using Equation (1).

$$X_n = \left(\frac{(b-a)}{(B-A)} \times X_{\text{unscaled}} \right) + \left(a - \left[A \times \frac{(b-a)}{(B-A)} \right] \right) \quad (1)$$

where A and B are the minimum and maximum values of the unscaled data set, respectively, and a and b are the minimum and maximum values of the scaled data set, respectively.

3.2. Overview of the Artificial Neural Network Model

3.2.1. Basic Concept of ANN

Artificial neural networks (ANNs) are complex mathematical models inspired by biological neurons, and they emulate biological neural networks. They are widely used for nonlinear system modeling and system identification [13]. A typical ANN consists of an input layer, one or more hidden layers, and an output layer. The numbers of layers and neurons in each layer depend on the complexity of the problem under consideration.

3.2.2. Mathematical Representation of ANN Architecture

A neural network in its simplest form can be used to model the relationship between data points x and the corresponding real-valued targets y . Mathematically, if our inputs (x) comprise n features, we can choose weights (w) and bias (b) such that our prediction (y') is given by Equation (2).

$$y' = w_1 \cdot x_1 + \dots + w_n \cdot x_n + b \quad (2)$$

For easy computation, all the features can be collected into a vector x and all weights into a vector w to express our model compactly using the dot product notation—Equation (3).

$$y' = w^T x + b \tag{3}$$

ANNs can learn by example (supervised learning). In ANNs, a set of input variables are multiplied by adjustable connection weights to produce the output. When input data are fed to an ANN, the ANN adjusts through a feed-forward back-propagation technique to determine the rules governing the relationship between the concerned variables. Figure 2 shows a graphical depiction of a typical feedforward ANN architecture. A neural network is trained using error back-propagation.

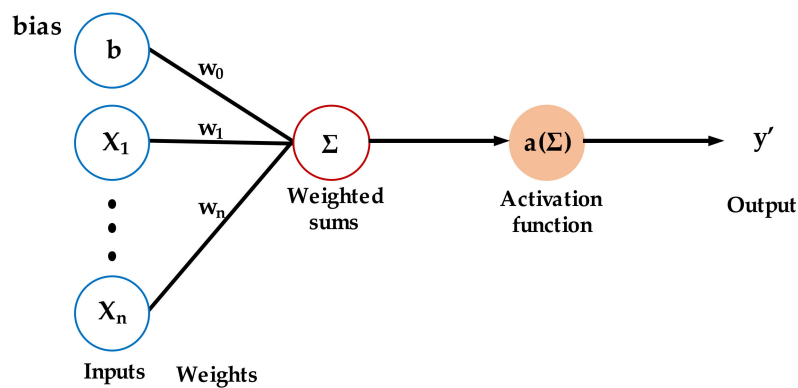


Figure 2. Feedforward neural network architecture.

Two ANN models were considered in this study, and they are shown in Figure 3. Both models had three input variables. The input variables of model 1 were unit weight (γ), corrected SPT blow count ($N_{1(60)}$), and cyclic stress ratio (CSR), while those of model 2 were depth of the soil layer (d), $N_{1(60)}$, and CSR.

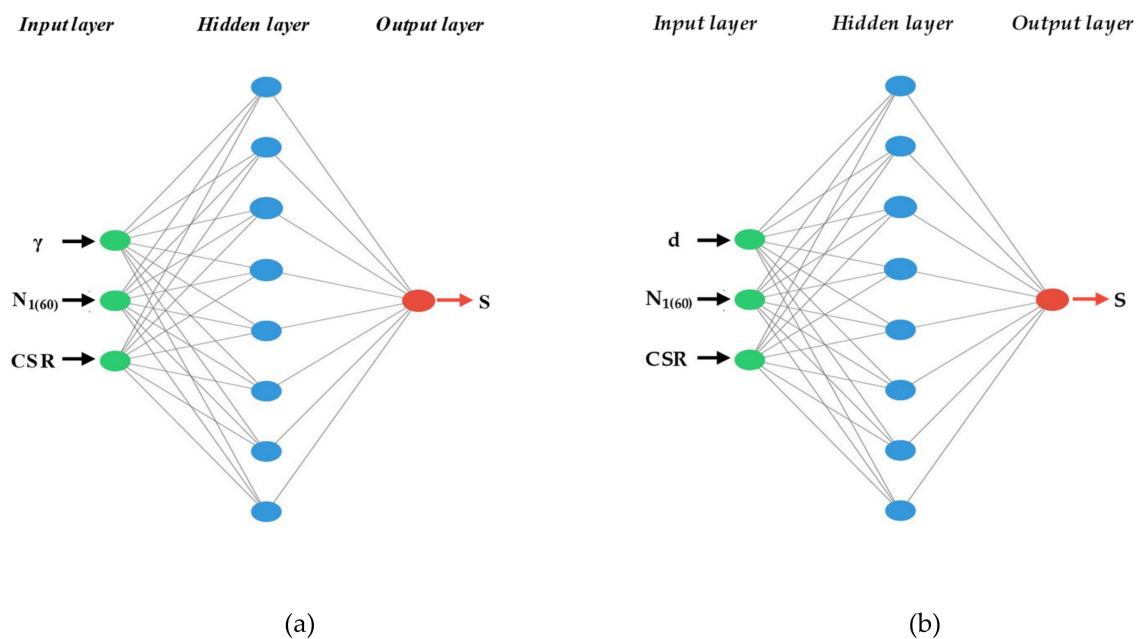


Figure 3. Architecture of the artificial neural network (ANN); (a) model 1 and (b) model 2.

The choice of input parameters was based on domain knowledge. They were chosen by considering how the seismic and soil properties influence liquefaction-induced settlement. The soil properties

considered were γ , $N_{1(60)}$, and d , while the CSR represented the seismic property. The CSR quantifies the demand imposed on the critical soil layer as a result of the seismic ground motion.

4. Results and Discussion

Table 2 summarizes the performance statistics of the two ANN models used for settlement prediction. For the test data set, models 1 and 2 had R^2 (coefficient of determination) values of 0.8601 and 0.7352 and MAE (mean of absolute errors) values of 0.1941 and 0.3136, respectively.

Table 2. Performance statistics of the ANN models.

Model	Input Parameters	Output	No. of Epochs	R^2	MAE
1	$\gamma, N_{1(60)}, CSR$	S	60	0.8601	0.1941
2	$d, N_{1(60)}, CSR$		60	0.7352	0.3136

After the models were trained, the root mean square error (RMSE) and loss were plotted to check the models' performance for the training and test data sets, as shown in Figures 4 and 5. The x -axis represents the number of epochs (i.e., the number of times the model ran through the entire training/test data set and updated the weights).

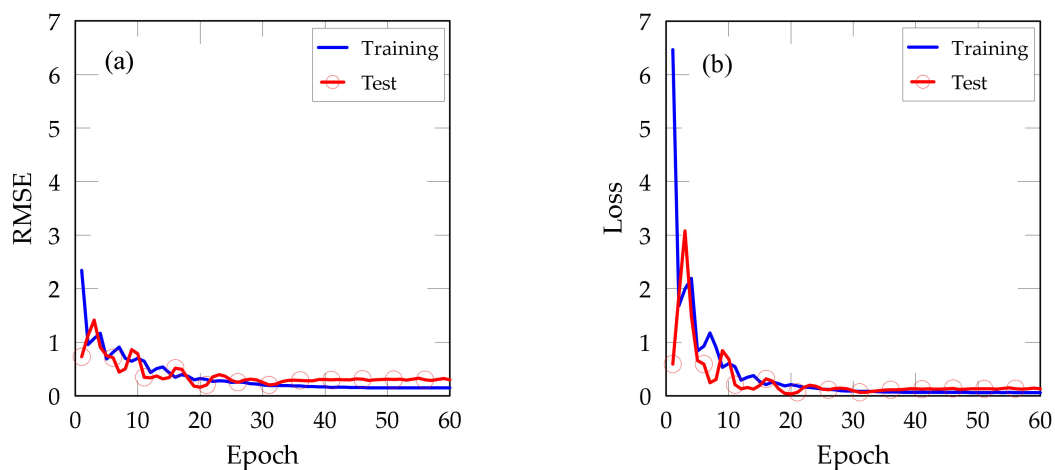


Figure 4. Plot of the (a) root mean square error (RMSE) and (b) loss for ANN model 1.

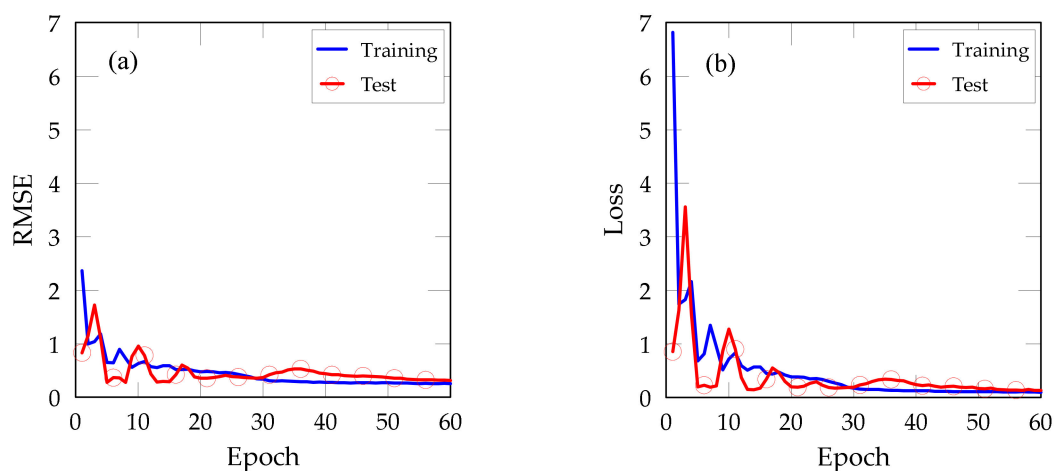


Figure 5. Plot of the (a) RMSE and (b) loss for ANN model 2.

Figures 6 and 7 show the performance of the ANN models in terms of R^2 for the test data set.

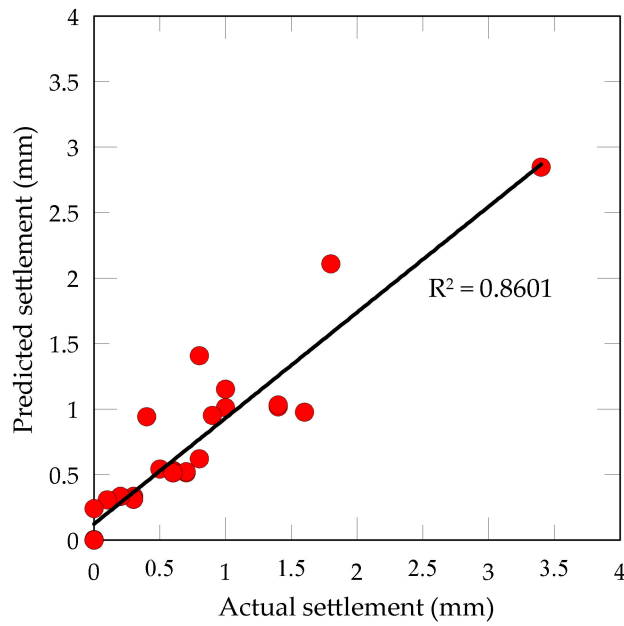


Figure 6. Scatter plot showing the performance of ANN model 1 for the test data set.

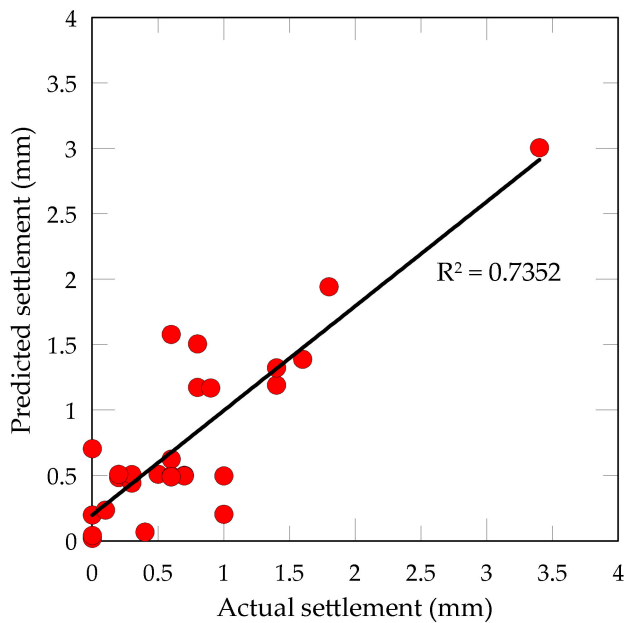


Figure 7. Scatter plot showing the performance of ANN model 2 for the test data set.

A comparison of models 1 and 2 in terms of the prediction accuracy shows that the prediction accuracy of the former is higher. The difference in the R^2 correlation between the two models is about 0.12.

From the results shown in Figures 5 and 6, it can be concluded that there exists a strong correlation between the model predictions and the actual settlement in both cases considered.

In this study, ANN models composed of two or more hidden layers were considered, and it was found that the difference in accuracy between models with two or more hidden layers and the model with the single hidden layer was not significant. Therefore, an ANN model using one layer was used.

4.1. ANN-Based Numerical Equation

A simple equation was developed to predict the liquefaction-induced settlement. The optimal ANN model structure used for the purpose is shown in Figure 8, and its associated weights with biases are presented in Table 3.

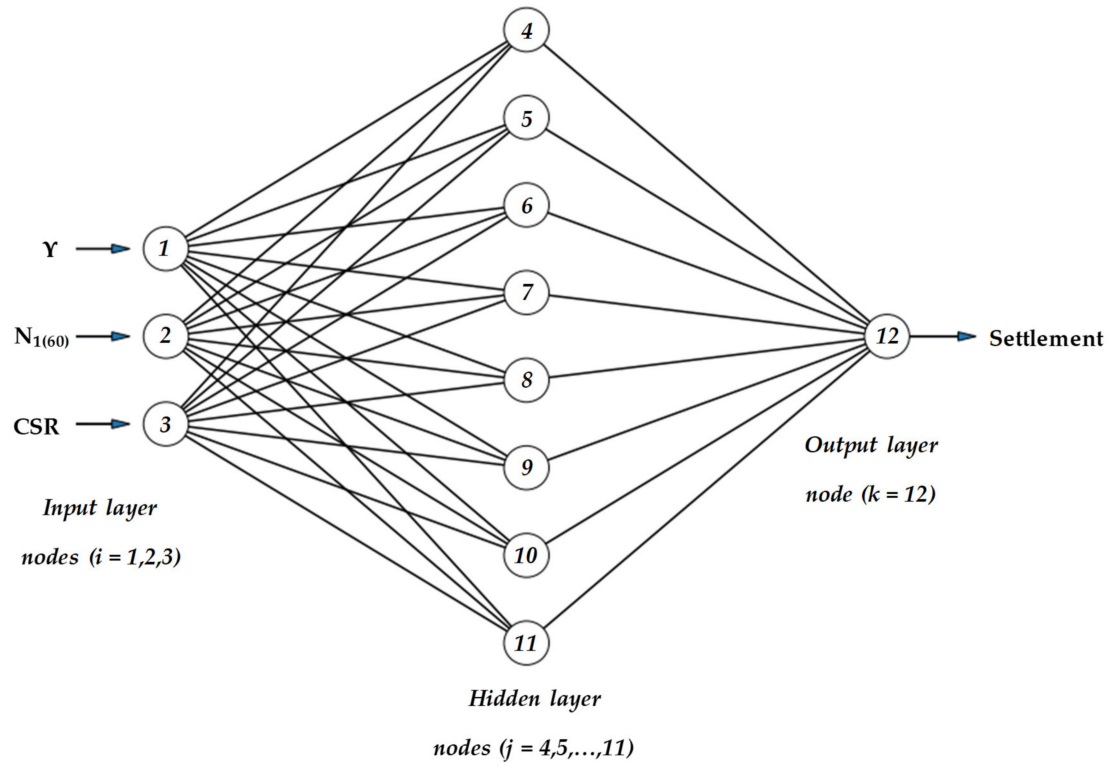


Figure 8. Structure of the optimal ANN model.

Table 3. Weight matrix and bias vector for the ANN model.

W₁		-2.231		2.729		-2.500		B₁	-9.631	
		-8.874		-3.629		-15.703			-6.179	
		-6.271		-5.433		-1.570			-5.334	
		-1.100		5.470		-3.295			-8.614	
		5.617		7.774		1.701			-7.317	
		-1.866		-4.224		-9.756			-0.926	
		-2.116		7.453		-1.157			-7.489	
		0.314		-1.285		-4.980			-6.722	
W₂	0.579	-1.853	-1.058	-1.591	1.006	1.964	-0.852	-0.320	B₂	1.006

Note: Matrices W₁ (8 × 3), B₁ (8 × 1), W₂ (1 × 8) and B₂ (1 × 1) were used in Equation (2)

The optimal-ANN-model-based numerical equation for settlement prediction can be expressed as Equation (4).

$$f_{sig} = \sigma(z) = \frac{1}{1 + e^{-z}} \tag{4}$$

where T₁₂ is the output variable, namely, the predicted settlement value (S), B_k is the bias value at the output layer, W_{kj} is the connection weight between the jth node in the hidden layer and the kth node in the output layer, B_j is the bias value of the jth hidden node, W_{ji} is the connection weight between

the i th input node and the j th hidden node, X_i is the i th input variable, and f_{sig} is the sigmoid transfer function given by Equation (5).

$$S = T_{12} = B_k + \sum_{j=4}^{11} \left\{ W_{kj} \times f_{sig} \left[B_j + \sum_{i=1}^3 (W_{ji} X_i) \right] \right\} \quad (5)$$

For the simplification of the calculation process, the weights and biases were arranged in a matrix form.

4.2. Example of Settlement Calculation Using the ANN Model

For $\gamma = 18 \text{ kN/m}^3$, $N_{1(60)} = 13$, and $\text{CSR} = 0.34$, the input vector \mathbf{X} is

$$\mathbf{X} = \begin{bmatrix} 18 \\ 13 \\ 0.34 \end{bmatrix}$$

The normalized input vector (X_n) is calculated from Equation (1) by using the A and B values in Table 1:

$$X_n = \begin{bmatrix} -0.200 \\ 0.040 \\ 0.444 \end{bmatrix}$$

Note: $(a, b) = (-1, 1)$

The settlement (S) is calculated using the normalized input vector as follows:

$$W_1 \times X_n + B_1 = \begin{bmatrix} -2.231 & 2.729 & -2.500 \\ -8.874 & -3.629 & -15.703 \\ -6.271 & -5.433 & -1.570 \\ -1.100 & 5.470 & -3.295 \\ 5.617 & 7.774 & 1.701 \\ -1.866 & -4.224 & -9.756 \\ -2.116 & 7.453 & -1.157 \\ 0.314 & -1.285 & -4.980 \end{bmatrix} \times \begin{bmatrix} -0.200 \\ 0.040 \\ 0.444 \end{bmatrix} + \begin{bmatrix} -9.631 \\ -6.179 \\ -5.334 \\ -8.614 \\ -7.317 \\ -0.926 \\ -7.489 \\ -6.722 \end{bmatrix} = \begin{bmatrix} -10.187 \\ -11.529 \\ -4.995 \\ -9.640 \\ -7.374 \\ -5.058 \\ -7.282 \\ -9.049 \end{bmatrix}$$

$$f_{sig}(W_1 \times X_n + B_1) = \begin{bmatrix} 3.76E-05 \\ 9.84E-06 \\ 6.73E-03 \\ 6.51E-05 \\ 6.27E-04 \\ 6.32E-03 \\ 6.87E-04 \\ 1.17E-04 \end{bmatrix}$$

$$S = [0.579 \quad -1.853 \quad -1.058 \quad -1.591 \quad -0.423 \quad 1.964 \quad -0.852 \quad -0.320]$$

$$\times \begin{bmatrix} 3.76 \times 10^{-5} \\ 9.84 \times 10^{-6} \\ 6.73 \times 10^{-3} \\ 6.51 \times 10^{-5} \\ 6.27 \times 10^{-4} \\ 6.32 \times 10^{-3} \\ 6.87 \times 10^{-4} \\ 1.17 \times 10^{-4} \end{bmatrix} + [1.006]$$

$$S = [1.010]$$

The actual value of the settlement was 1 mm, and the value predicted using the ANN model was 1.010 mm.

4.3. Sensitivity Analysis

Sensitivity analysis was performed to determine the effect of the input parameters on the settlement prediction. The measure of variable importance was obtained using the permutation importance approach for random forests, described by Breiman [14]. This approach involves measuring the drop in the ANN model performance when a feature is unavailable.

As shown in Figures 9 and 10, the unit weight had the strongest influence on the settlement prediction in the case of ANN model 1, while the depth of the soil layer had the strongest influence on the predicted settlement in the case of model 2. In both cases, $N_{1(60)}$ had a stronger influence than the CSR.

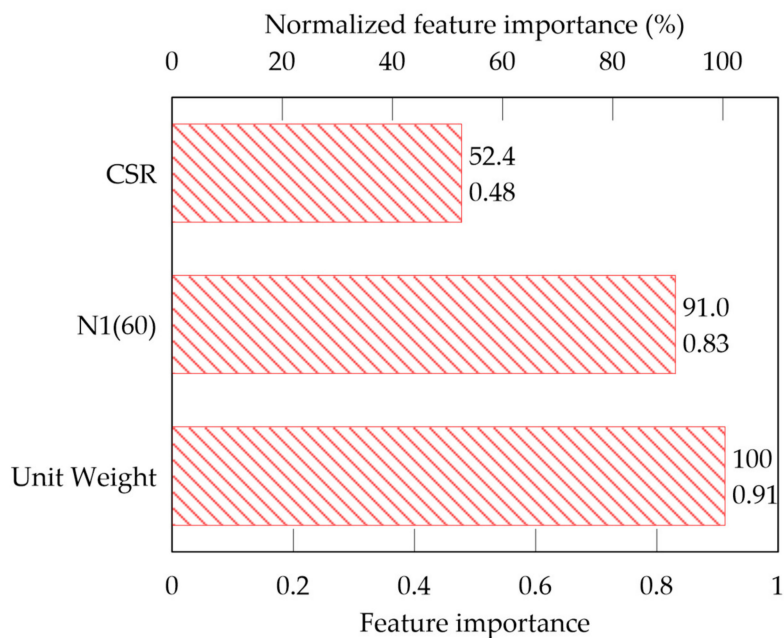


Figure 9. Relative importance of the input parameters of ANN model 1.

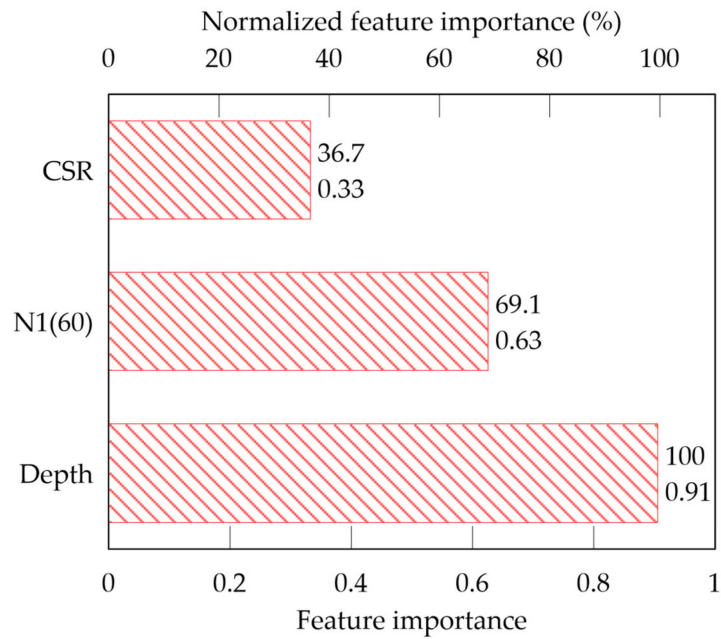


Figure 10. Relative importance of the input parameters of ANN model 2.

4.4. Parametric Study and Extrapolation beyond the Training Data

A parametric study was conducted to verify the validity and robustness of the optimal ANN model, and it involved generating a synthetic data set within the range of the training data set to test the model. For a given unit weight of soil, the settlement was determined based on the unit thickness of each layer. As shown in Figure 11a, the amount of predictive settlement generally increased with increasing a CSR and decreased with an increase in $N_{1(60)}$. However, it is necessary to expand the range of $N_{1(60)}$ and CSR obtained through the parametric study due to some field data being beyond the range. Therefore, this study proposed a simple settlement chart based on a parametric study as shown in Figure 11b.

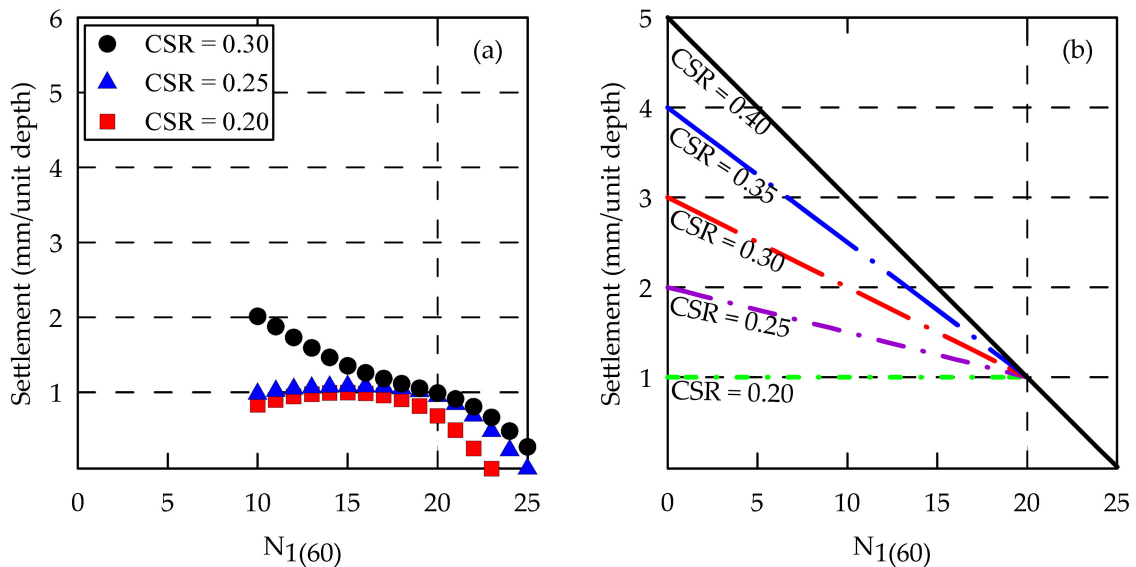


Figure 11. Variation of settlement with $(N_1)_{60}$ and CSR for $\gamma = 18 \text{ kN/m}^3$. (a) Settlement relationship between $(N_1)_{60}$ and CSR; (b) settlement chart based on the ANN method.

4.5. Application of Settlement Chart Based on the ANN Method

The proposed settlement chart from the optimal ANN model was assessed using the SPT data obtained from three additional boreholes at the Pohang site. The locations of the boreholes and the measured settlement obtained from interferometric synthetic aperture radar (InSAR) imaging are shown in Figure 12.

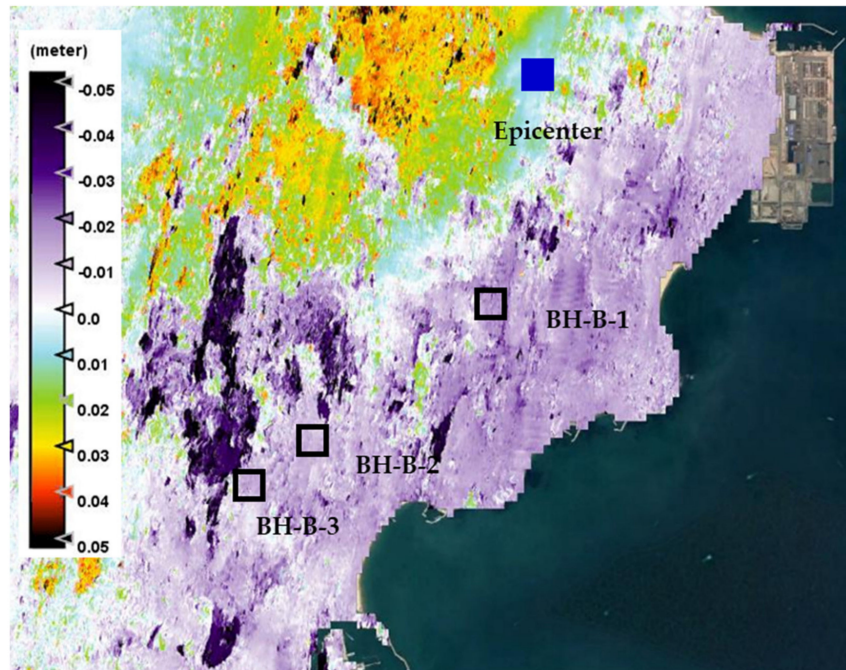


Figure 12. A settlement map from interferometric synthetic aperture radar (InSAR) and a location of extra boreholes (BHs).

The InSAR procedure was recommended by the Remote Sensing Lab at Kangwon National University, Korea [15]. Following the procedure, the settlement was analyzed by the Pohang satellite images between November 4 and 16, 2017, from Google Earth. Such Google Earth images were used to generate the settlement map in Figure 12 by using a freely distributed SentiNel Application Platform (SNAP) program by the European Space Agency [16]. With an average unit weight of 18 kN/m^3 , $N_{1(60)}$ values were converted from the SPT blow count (N_{SPT}) of boreholes [17]. The CSR can be calculated from Equation (6) [18].

$$CSR = (\tau_{av} / \sigma'_{vo}) = 0.65(a_{max} / g)(\sigma_{vo} / \sigma'_{vo})\gamma_d \quad (6)$$

where a_{max} = peak acceleration at the ground surface from the earthquake (this study used the Pohang Earthquake, 0.2712 g); g = acceleration of gravity; σ_{vo} and σ'_{vo} are total and effective vertical overburden stresses, respectively; and γ_d = stress reduction coefficient.

The calculated total settlement for the additional boreholes, 1, 2, and 3, using the optimal ANN model are 17.14, 19.77, and 13.88 mm, respectively, as shown in Table 4. It can be observed that these settlement values are close to those measured by the InSAR imaging. Unlike the numerical analysis approach, the proposed chart between $(N_1)_{60}$ -CSR-Settlement from the optimal ANN model has been proven to estimate settlement values with minimal input parameters. For an earthquake with similar impact and magnitude, this simple ANN model can be deployed as a handy tool to obtain liquefaction-induced settlement in the field.

Table 4. Predicted settlement due to Pohang earthquake using the proposed settlement chart.

Depth	BH-B-1				BH-B-2				BH-B-3			
	N _{spt}	(N ₁) ₆₀	CSR	S(mm)	N _{spt}	(N ₁) ₆₀	CSR	S(mm)	N _{spt}	(N ₁) ₆₀	CSR	S(mm)
0	3	4	0.39	4.04	4	7	0.39	3.47	4	6	0.39	3.66
1	4	5	0.39	3.85	5	8	0.39	3.28	14	23	0.39	0.4
2	5	8	0.39	3.28	6	10	0.39	2.9	7	11	0.39	2.71
3	7	11	0.39	2.71	7	12	0.39	2.52	7	11	0.39	2.71
4	9	14	0.38	2.08	9	13	0.38	2.26	8	12	0.38	2.44
5	13	19	0.38	1.18	10	13	0.38	2.26	13	18	0.38	1.36
6	21	28	0.38	0	11	14	0.38	2.08	17	22	0.38	0.6
7	29	36	0.37	0	17	20	0.37	1	21	25	0.37	0
8	37	43	0.37	0	42	48	0.37	0	24	27	0.37	0
9	44	49	0.36	0	36	39	0.36	0	28	31	0.36	0
10	50	53	0.35	0	50	53	0.35	0	47	50	0.35	0
11									50	51	0.34	0
	Total Settlement			17.14	Total Settlement			19.77	Total Settlement			13.88

5. Conclusions

In this study, the potential of an ANN to predict the liquefaction-induced settlement at Pohang was examined. Two ANN models were trained using a back-propagation algorithm. Both models had three input variables. The input variables of model 1 were unit weight, corrected SPT blow count ($N_{1(60)}$), and CSR, while those of model 2 were depth of the soil layer, $N_{1(60)}$, and CSR. The output of the models was the settlement (S). After the training and testing of the models, it was evident that model 1 had higher prediction accuracy, and the difference in the R^2 correlation between the two models was about 0.12. Subsequently, the weights and biases of an optimal ANN model were used to develop a simple predictive model equation, which was implemented using a matrix formulation.

Sensitivity analysis performed using the permutation importance algorithm indicated that the corrected SPT blow count had a stronger influence than the CSR on the predicted settlement. Furthermore, a parametric study showed that for a given unit weight of soil, the settlement decreased with an increase in $N_{1(60)}$.

Finally, the simplified relationship between $(N_1)_{60}$ -CSR-Settlement was proposed using the optimal ANN model, and the cumulative settlement was predicted by applying the proposed relationship to additional boreholes and compared with the InSAR results. The cumulative settlement had a similar range as the InSAR displacement map. Thus, the simplified relationship of this study can be deployed as a handy tool to obtain liquefaction-induced settlement in the field.

Author Contributions: Conceptualization, S.-S.P. and P.D.O.; methodology, S.-S.P. and P.D.O.; software, P.D.O. and S.-W.W.; validation, S.-S.P., P.D.O., and S.-W.W.; formal analysis, P.D.O., S.-S.P., and D.-E.L.; investigation, P.D.O. and S.-S.P.; resources, S.-S.P. and P.D.O.; data curation, S.-S.P. and P.D.O.; writing—original draft preparation, S.-S.P. and P.D.O.; writing—review and editing, S.-S.P. and P.D.O.; visualization, P.D.O. and S.-W.W.; supervision, S.-S.P.; project administration, S.-S.P. and D.-E.L.; funding acquisition, S.-S.P. All authors have read and agreed to the published version of the manuscript.

Funding: This work was supported by a National Research Foundation of Korea (NRF) grant funded by the Korean government (MSIT) (No. NRF-2018R1A5A1025137).

Conflicts of Interest: The authors declare no conflicts of interest.

Appendix A

Table A1. Details of the liquefaction-induced settlement database.

Borehole	Depth (m)	Unit Weight (kN/m ³)	N ₁₍₆₀₎	CSR	Settlement (mm)
BH-A-1	1	20	11	0.33	0.50
	2	20	11	0.31	0.50
	3	20	14	0.29	0.80
	4	20	16	0.28	1.40
	5	20	5	0.27	3.30
	6	20	10	0.26	3.40
	7	20	5	0.27	3.40
	8	20	6	0.29	2.50
	9	20	9	0.3	1.60
	10	20	9	0.31	1.00
	11	18	25	0.31	0.40
	12	18	25	0.31	0.30
	13	18	25	0.32	0.20
	14	18	25	0.32	0.30
	15	18	25	0.32	0.30
	16	18	25	0.32	0.30
	17	18	25	0.32	0.30
	18	18	25	0.32	0.20
	19	18	25	0.31	0.30
	20	18	25	0.31	0.30
BH-A-2	1	20	15	0.35	0.40
	2	20	17	0.32	0.80
	3	20	17	0.3	1.60
	4	20	7	0.29	3.10
	5	20	6	0.27	2.80
	6	21	13	0.31	1.40
	7	21	18	0.34	0.80
	8	21	13	0.36	0.90
	9	21	11	0.37	1.10
	10	21	13	0.36	0.80
	11	16	2	0.36	0.00
	12	16	1	0.37	0.00
	13	16	1	0.38	0.00
	14	16	1	0.39	0.00
	15	16	1	0.39	0.00
	16	16	1	0.39	0.00
	17	16	1	0.39	0.00
	18	16	1	0.39	0.00
	19	16	1	0.38	0.00
	20	16	1	0.37	0.00

Table A1. Cont.

Borehole	Depth (m)	Unit Weight (kN/m ³)	N ₁₍₆₀₎	CSR	Settlement (mm)
BH-A-3	1	18	6	0.24	0.60
	2	18	8	0.28	1.40
	3	18	10	0.3	2.00
	4	18	10	0.29	2.30
	5	18	11	0.28	2.00
	6	18	10	0.3	1.80
	7	18	11	0.32	1.40
	8	18	11	0.33	1.30
	9	18	12	0.34	1.20
	10	18	13	0.34	1.00
	11	21	25	0.34	0.70
	12	21	25	0.33	0.60
	13	21	25	0.33	0.60
	14	21	25	0.33	0.50
	15	21	25	0.32	0.50
	16	21	25	0.32	0.40
	17	21	25	0.31	0.50
	18	21	25	0.31	0.40
	19	21	25	0.3	0.40
	20	21	25	0.3	0.50
BH-A-4	1	20	5	0.23	1.10
	2	20	7	0.27	1.90
	3	20	18	0.27	1.60
	4	20	9	0.27	2.80
	5	20	6	0.26	2.80
	6	20	11	0.31	1.60
	7	20	9	0.34	1.40
	8	21	25	0.36	0.60
	9	21	25	0.38	0.60
	10	21	25	0.38	0.60
	11	21	25	0.38	0.60
	12	21	25	0.37	0.50
	13	16	7	0.22	0.00
	14	16	1	0.21	0.00
	15	16	0	0.21	0.00
	16	16	2	0.22	0.00
	17	16	3	0.22	0.00
	18	16	3	0.22	0.00
	19	16	3	0.22	0.00
	20	16	3	0.22	0.00

Table A1. Cont.

Borehole	Depth (m)	Unit Weight (kN/m ³)	N ₁₍₆₀₎	CSR	Settlement (mm)
BH-A-5	1	20	11	0.32	0.50
	2	20	10	0.31	1.60
	3	20	9	0.29	2.60
	4	20	11	0.3	1.90
	5	20	11	0.32	1.50
	6	20	10	0.33	1.40
	7	20	15	0.34	0.90
	8	20	15	0.35	0.80
	9	21	25	0.34	0.60
	10	21	25	0.34	0.60
	11	21	25	0.34	0.60
	12	21	25	0.33	0.60
	13	21	25	0.33	0.70
	14	21	25	0.33	0.70
	15	18	15	0.33	1.10
	16	18	11	0.33	1.40
	17	18	12	0.32	1.00
	18	16	14	0.32	0.10
	19	16	10	0.32	0.00
	20	16	7	0.32	0.00

References

- Choi, J.H.; Ko, K.; Gihm, Y.S.; Cho, C.S.; Lee, H.; Song, S.G.; Bang, E.S.; Lee, H.J.; Bae, H.K.; Kim, S.W.; et al. Surface Deformations and Rupture Processes Associated with the 2017 Mw 5.4 Pohang, Korea, Earthquake. *Bull. Seismol. Soc. Am.* **2019**, *109*, 756–769. [CrossRef]
- Gihm, Y.S.; Kim, S.W.; Ko, K.; Choi, J.-H.; Bae, H.; Hong, P.S.; Lee, Y.; Lee, H.; Jin, K.; Choi, S.; et al. Paleo seismological implications of liquefaction-induced structures caused by the 2017 Pohang Earthquake. *Geosci. J.* **2018**, *22*, 871–880. [CrossRef]
- Kang, S.; Kim, B.; Bae, S.; Lee, H.; Kim, M. Earthquake-Induced Ground Deformations in the Low-Seismicity Region: A Case of the 2017 M5.4 Pohang, South Korea, Earthquake. *Earthq. Spectra* **2019**, *35*, 1235–1260. [CrossRef]
- Kim, H.-S.; Sun, C.-G.; Cho, H.-I. Geospatial Assessment of the Post-Earthquake Hazard of the 2017 Pohang Earthquake Considering Seismic Site Effects. *ISPRS Int. J. Geo-Inf.* **2018**, *7*, 375. [CrossRef]
- Naik, S.P.; Kim, Y.-S.; Kim, T.; Su-Ho, J. Geological and Structural Control on Localized Ground Effects within the Heunghae Basin during the Pohang Earthquake (Mw 5.4, 15th November 2017), South Korea. *Geosciences* **2019**, *9*, 173. [CrossRef]
- National Academies of Sciences, Engineering, and Medicine. *State of the Art and Practice in the Assessment of Earthquake-Induced Soil Liquefaction and Its Consequences*; The National Academies Press: Washington, DC, USA, 2016.
- Da Fonseca, A.V.; Millen, M.; Gómez-Martínez, F.; Romão, X.; Quintero, J. State of the Art Review of Numerical Modelling Strategies to Simulate Liquefaction-Induced Structural Damage and of Uncertain/Random Factors on the Behaviour of Liquefiable Soils. Deliverable D3.1, Version 1.0. 2017. Available online: <http://www.liquefact.eu/disseminations/deliverables/> (accessed on 11 January 2020).
- Tang, X.-W.; Hu, J.-L.; Qiu, J.-N. Identifying significant influence factors of seismic soil liquefaction and analyzing their structural relationship. *KSCE J. Civ. Eng.* **2016**, *20*, 2655–2663. [CrossRef]
- Lee, C.Y.; Chern, S.-G. Application of a Support Vector Machine for Liquefaction Assessment. *J. Mar. Sci. Technol.* **2013**, *21*, 318–324. [CrossRef]

10. Xue, X.; Liu, E. Seismic liquefaction potential assessed by neural networks. *Environ. Earth Sci.* **2017**, *76*, 192. [[CrossRef](#)]
11. Integrated DB Center of National Geotechnical Information, SPT Database Available at 542. 2015. Available online: <http://www.geoinfo.or.kr> (accessed on 15 May 2015).
12. Park, S.S. Liquefaction evaluation of reclaimed sites using an effective stress analysis and an equivalent linear analysis. *KSCE J. Civ. Eng.* **2008**, *28*, 83–94.
13. Lai, J.; Qiu, J.; Feng, Z.; Chen, J.; Fan, H. Prediction of Soil Deformation in Tunnelling Using Artificial Neural Networks. *Comput. Intell. Neurosci.* **2016**, *2016*, 6708183. [[CrossRef](#)]
14. Breiman, L. Random Forests. *Mach. Learn.* **2001**, *45*, 5–32. [[CrossRef](#)]
15. Lee, H.Y. Pohang Earthquake (15 November 2017 Mw 5.4) observed by Sentinel-1A/B SAR Interferometry. Available online: <http://sar.kangwon.ac.kr/pohang.htm> (accessed on 11 December 2017).
16. Fomelis, M.; Blasco, J.M.D.; Desnos, Y.L.; Engdahl, M.; Fernández, D.; Veci, L.; Lu, J.; Wong, C. ESA SNAP-StaMPS Integrated Processing for Sentinel-1 Persistent Scatterer Interferometry. In Proceedings of the IGARSS 2018—2018 IEEE International Geoscience and Remote Sensing Symposium, Valencia, Spain, 22–27 July 2018; pp. 1364–1367. [[CrossRef](#)]
17. Youd, T.L.; Idriss, I.M. Liquefaction resistance of soils: Summary report from the 1996 NCEER and 1998 NCEER/NSF workshops on evaluation of liquefaction resistance of soils. *J. Geotech. Geoenvironmental Eng.* **2001**, *127*, 297–313. [[CrossRef](#)]
18. Seed, H.B.; Idriss, I.M. Simplified procedure for evaluating soil liquefaction potential. *J. Soil Mech. Found. Div.* **1971**, *97*, 1249–1273.



© 2020 by the authors. Licensee MDPI, Basel, Switzerland. This article is an open access article distributed under the terms and conditions of the Creative Commons Attribution (CC BY) license (<http://creativecommons.org/licenses/by/4.0/>).